Influence of Fullerene Multiadducts on the Morphology and Charge Photogeneration of Their Photovoltaic Blends with Poly(3-hexylthiophene)

ARTICLE *in* THE JOURNAL OF PHYSICAL CHEMISTRY C · JANUARY 2013

Impact Factor: 4.77

6 AUTHORS, INCLUDING:

Wei Zhang

Lund University

18 PUBLICATIONS **13** CITATIONS

SEE PROFILE

Jian-Ping Zhang

Renmin University of China

144 PUBLICATIONS **2,027** CITATIONS

SEE PROFILE

Xiao-Feng Wang

Jilin University

44 PUBLICATIONS **835** CITATIONS

SEE PROFILE

THE JOURNAL OF PHYSICAL CHEMISTRY C

Article

pubs.acs.org/JPCC

Influence of Fullerene Multiadducts on the Morphology and Charge Photogeneration of Their Photovoltaic Blends with Poly(3-hexylthiophene)

Yu-Wei Wang,[†] Wei Zhang,[†] Xi-Cheng Ai,[†] Jian-Ping Zhang,*[,†] Xiao-Feng Wang,[‡] and Junji Kido[‡]

[†]Department of Chemistry, Renmin University of China, Beijing 100872, People's Republic of China

[‡]Research Center for Organic Electronics (ROEL), Graduate School of Engineering, Yamagata University, 4-3-16 Jonan, Yonezawa, Yamagata 992-8510, Japan

Supporting Information

ABSTRACT: A series of benzene octyl ether adducted fullerene derivatives (PCBOEs) of higher LUMO levels with reference to PCBM were synthesized and were blended with P3HT to assemble polymer solar cells (PSCs). Upon increasing the adduct order, the PCBOE-based PSCs exhibited higher open-circuit voltage (V_{OC}) but increasingly lower short-circuit current density (J_{SC}) with respect to the P3HT:PCBM device. Morphological analyses of the P3HT:fullerene blends reveal different extents of fullerene aggregation, which are shown to impact intimately on the charge photogeneration dynamics. An increase of adduct order is found to accelerate geminate charge recombination and to induce nanosecond nongeminate charge recombination that is absent in the cases of monoadducted PCBOE and PCBM. The severer charge recombination found for higher order fullerene adducts is ascribed to the deterioration of electron mobility owing to the discontinuity of the fullerene phase. The results suggest that, upon increasing the adduct order, the electron and hole transport in photoactive layers turn from ambipolarly balanced to space-charge limited states, a crucial issue for the application of multiadducted fullerenes as the electron accepting materials of PCSs.

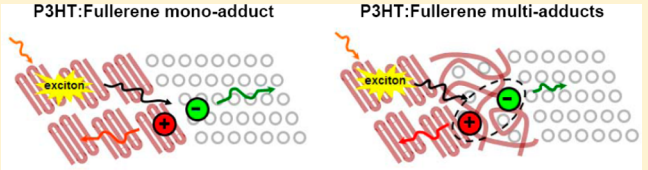

1. INTRODUCTION

Over the past decade, polymer solar cells (PSCs) have been attracting extensive academic and industrial interests owing to the merits of solution processability, low cost, low weight, and device flexibility. To improve the light-to-electrical power conversion efficiency (PCE), the bulk heterojunction (BHJ) configuration of photoactive layers has been widely adopted, which maximizes the interfaces between the electron donor and acceptor materials for efficient exciton dissociation into charge carriers.[1−4] A BHJ photoactive layer with a typical thickness of a few tens to a hundred nanometers comprises the bicontinuous interpenetrating network of the *p*-type conjugated polymer and the *n*-type fullerene derivative.[5−10] With reference to the homopolymers such as poly(phenylenevinylene) (PPV) and poly(3-hexylthiophene) (P3HT), low-bandgap copolymers with extended light-harvesting spectral range are promising in simultaneously boosting the open-circuit voltage (V_{OC}) and the short-circuit current density (J_{SC}), and hence in improving the PCE.[11−14] Among various types of PSCs, those based on the electron-donating P3HT mixed with the electron accepting [6,6]-phenyl-C_{61}-butyric acid methyl ester (PCBM) show a moderate PCE of 4−7% with good reproducibility.[15−20] Hence, the P3HT−PCBM combination has been an archetypical PSC model system with a wealthy accumulation of understanding in the structure−activity relationship of light conversion.[19,21,22]

Fullerene derivatives $PC_{61}BM$ and $PC_{71}BM$ have been widely adopted for PSCs owing to the high electron affinity and the excellent solubility in a range of organic solvents. Since the key device parameter V_{OC} relies on the difference between the energy levels of the highest occupied molecular orbital (E_{HOMO}) of polymer and the lowest unoccupied molecular orbital (E_{LUMO}) of fullerene, a higher E_{LUMO} of fullerene enables a larger V_{OC} and, concomitantly, reduces the free energy loss of the usable electrons.[23−25] To this end, a range of novel fullerene derivatives with distinctive structural variation were devised, for example, those with electron-donating groups in the phenyl ring of PCBM,[26−28] fullerene multiadducts[29−33] and endohedral fullerenes,[34] and so forth. In general, the strategy of raising fullerene E_{LUMO} has succeeded in enhancing V_{OC} but has hardly been effective in improving J_{SC}. Therefore, seeking for novel electron-accepting fullerene materials for PCE enhancement remains a challenging task.[35−38] Recently, the solvent solubility and the polymer miscibility of fullerene adducts have been shown to be highly influential on the morphology of a photoactive layer.[39−41] Meanwhile, to clarify the structure−activity relationship of the fullerene-adduct-based PSCs, charge photogeneration dynamics have been investigated in connection with the film morphology and the charge mobility.[42−45]

The present work is intended to investigate the effects of film morphology and charge transport on the subnanosecond

Received: August 9, 2013
Revised: November 20, 2013
Published: November 21, 2013

charge photogeneration and recombination dynamics in the photoactive blends of P3HT with fullerene adducts. We have newly synthesized three fullerene derivatives including the monoadducted 4-(pentyl-[6,6]-C_{61})-benzene octyl ether (mono-PCBOE), the bis-adducted 4-(pentyl-[6,6]-C_{61})-benzene octyl ether (bis-PCBOE), and the tris-adducted 4-(pentyl-[6,6]-C_{61})-benzene octyl ether (tris-PCBOE) (Scheme 1), and

Scheme 1. Molecular Structures of P3HT, PCBM and the Fullerene Adducts Mono-PCBOE, Bis-PCBOE, and Tris-PCBOE

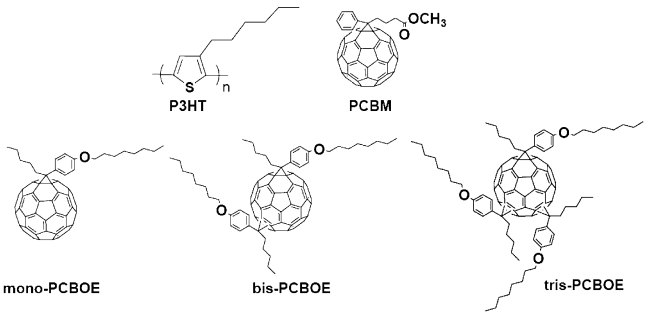

we have compared the performance among the P3HT:mono-PCBOE, the P3HT:bis-PCBOE, and the P3HT:tris-PCBOE devices with reference to the classical P3HT:PCBM device. The photoactive layers were all processed by slow drying followed by thermal annealing,[17] so as to ensure that the P3HT phases in different types of photoactive layers are of similar crystallinity. In this way, the influence of fullerene adducts on the film morphology and the charge photogeneration dynamics can be underlined. Detailed morphological and time-resolved spectroscopic studies show that bis-PCBOE and tris-PCBOE with higher adduct orders aggravate geminate and nongeminate charge recombination owing to the poor electron mobility originating from the discontinuity of fullerene phases. It is concluded that, on going from the mono- to the tris-adduct, the transport of electrons and holes turns from ambipolarly balanced to space-charge limited states. This work points to the utmost importance of the balanced flow of charge carriers in photoactive layers, which is crucial for the success in using fullerene multiadducts for efficient PSCs.

2. MATERIALS AND METHODS

2.1. Materials and Synthetic Route. P3HT and PCBM were purchased from Sigma-Aldrich, Co, and *o*-Dichlorobenzene (*o*-DCB) was obtained from Alfa-Aesar Company. Other chemicals and solvents were purchased from Beijing Chemical Company. Synthesis of the fullerene adducts (Scheme 1) with reported methods[46] are briefly described below with reference to the route in Scheme 2. *n*-Octyl phenyl ether (**1**) was synthesized from phenol by etherification with 1-bromooctane, which was successively converted to 4-octyloxy hexanophenone (**2**) and 4-octyloxy hexanophenone tosylhydrazone (**3**). The final step was a one-pot reaction with **3** and C_{60} in *o*-DCB refluxed for 12 h at 140 °C. The target fullerene adducts, unreacted C_{60}, and other C_{60} multiadducts comprised the products. The desired mono-PCBOE, bis-PCBOE, and tris-PCBOE were purified via several repeats of silica gel column chromatography with toluene/*n*-hexane (1:9, v/v) as eluent. More synthetic details and ^{1}H NMR, ^{13}C NMR (for mono-PCBOE), and MS (MALDI-TOF) data for structural characterization are given in Supporting Information S1.

2.2. Device Fabrication and Characterization. The PSCs were configured as ITO|PEDOT:PSS (25 nm)|P3HT:fullerene derivative (160 nm)|Ca (20 nm)|Al (100 nm). Patterned ITO substrates with the sheet resistance of 15 Ω per square were purchased from Lumtec, which were precleaned with detergent, ultrasonicated in deionized water, acetone, and isopropyl alcohol, and subsequently ultraviolet-ozone treated for 30 min. The PEDOT:PSS layers were spin-coated onto the pretreated ITO substrates. The *o*-DCB solutions of P3HT-fullerene mixtures (1:1, w/w; total concentration, 40 mg/mL) were spin-coated on the PEDOT:PSS layers (700 rpm), and the wet films were then dried in covered Petri dishes (45 min) before being subjected to thermal annealing (110 °C, 10 min).[17] The Ca and Al layers were thermally deposited in turn ($<1 \times 10^{-5}$ Pa). The thickness of photoactive layers was determined with a DEKTAK surface profilemeter. The device photoactive areas were 4 mm^2. External quantum efficiency (EQE) and PCE were measured with a CEP-2000 integrated system (Bunkou Keiki) under standard conditions, and each set of data was an average over four independent devices. The electron mobility was derived from the electron single-carrier devices configured as ITO|Ca (1 nm)|fullerene derivative (200 nm)|Ca (20 nm)|Al (100

Scheme 2. Synthetic Routes of Mono-PCBOE, Bis-PCBOE, and Tris-PCBOE

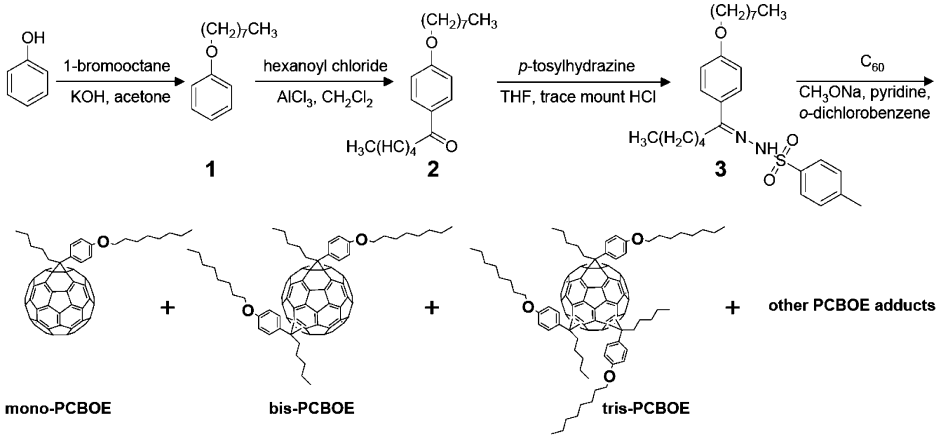

dx.doi.org/10.1021/jp407990d | J. Phys. Chem. C 2013, 117, 25898−25907

nm)[47] according to the theory of space-charge limited current (SCLC).[48]

2.3. Spectroscopic and Morphological Characterization. UV−visible absorption spectra were measured on a Cary 50 absorption spectrometer (Varian Inc., Palo Alto, CA)). The cyclic voltammograms of PCBM, mono-PCBOE, bis-PCBOE, and tris-PCBOE in *o*-DCB-acetonitrile binary solvent (5:1, v:v) with 0.1 M tetrabutylammonium perchlorate (Bu_4NClO_4) were scanned on an electrochemical workstation (100 mV/s; Epsilon BAS, Bioanalytical Systems, Inc., West Lafayette, IN), for which a three-electrode configuration was used: a glassy carbon working electrode (diameter, 3 mm), a platinum counter electrode, and an Ag/Ag^+ reference electrode (0.1 M $AgNO_3$, 0.1 M Bu_4NClO_4 in *o*-DCB and acetonitrile (5:1, v:v)). The AFM images were taken with tapping mode in air at room temperature (Veeco, D3100). The near-infrared time-resolved absorption spectrometer, described in detail elsewhere,[49,50] was operated in multicolor detection mode (850−1350 nm) with a temporal resolution of 160 fs and an ΔOD detection sensitivity better than 10^{-4}.

3. RESULTS AND DISCUSSION

3.1. Spectroscopic, Cyclic Voltammetric, and Morphological Characterizations. Figure 1 shows the UV−visible

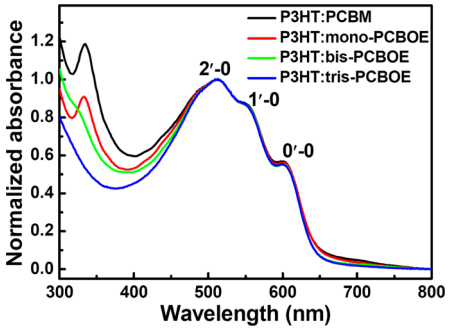

Figure 1. Normalized absorption spectra of P3HT:PCBM and P3HT:PCBOE blend films processed with slow drying followed by thermal annealing.

absorption spectra of different blend films, among which no significant difference in the vibronic bands are seen (2′-0, 1′-0, 0′-0), indicating that the crystallinity of P3HT phases in the blends are similar probably owing to the slow solidification.[51] This is corroborated by the similar peak widths (~0.69°−0.70°, full width at half-maximum) of the X-ray diffraction patterns characteristic to the P3HT crystallites (Supporting Information S2). With reference to the P3HT:PCBM film, the P3HT:PCBOE films show declined absorption in 300−400 nm, which are ascribable to the decreased absorption of the fullerene adducts in this spectral region (Supporting Information S3). In Figure 1, the slightly weaker absorption of the P3HT:tris-PCBOE blend in 650−700 nm may be due to the change of electronic structure of tris-PCBOE induced by high-order adduction.

Figure 2 depicts the cyclic voltammograms of mono-PCBOE, bis-PCBOE, and tris-PCBOE dissolved in the binary solvent of *o*-DCB and acetonitrile (5:1, v/v), from which the reductive half-wave potentials were derived (E_i, i = 1, 2, 3; Table 1). With reference to PCBM, the reduction waves of PCBOEs shift systematically to higher potentials in the order of mono-PCBOE < bis-PCBOE < tris-PCBOE, and so do the onsets of

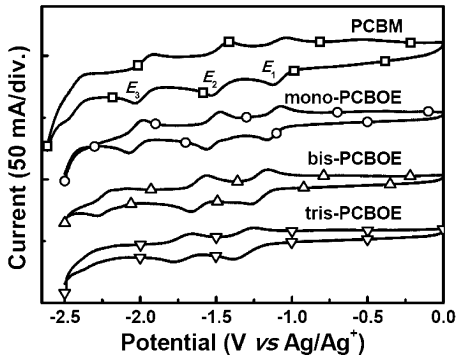

Figure 2. Cyclic voltammograms scanned at 100 mV/s for PCBM and PCBOEs dissolved in the *o*-DCB-acetonitrile binary solvent (5:1, v/v).

the reduction potentials (E_{red}^{on}). In the potential regime of (−2.6 − 0.0) V, PCBM, mono-PCBOE, and bis-PCBOE exhibit three reversible waves, whereas tris-PCBOE shows two. For mono-PCBOE, the reduction potentials are slightly more negative than those of PCBM, which is attributed to the inductive effect of the side-chain phenyl substituted with an electron-donating alkoxyl lying parallel to the fullerene cage.[52] Such phenomena are well-known for fullerenes adducted with the side chains containing a phenyl ring[26] or a thienyl ring[31] attached with electron-donating groups. With reference to the monoadduct, the reduction potentials of higher adducts, bis-PCBOE and tris-PCBOE, shift further to the negative because of the additional shrinkage of π-conjugation and release of strain energy of the fullerene moieties.[31] For the same reasons, the E_{LUMO} levels deducted on the basis of the relation, $E_{LUMO} = -e(E_{red}^{on} + 4.71)$,[53] increased for 0.03 eV (mono-PCBOE), 0.12 eV (bis-PCBOE), and 0.21 eV (tris-PCBOE) with reference to PCBM (Table 1). For energetics consideration, a higher E_{LUMO} may lead to a higher V_{OC} of PSC.

The upper row of Figure 3 shows the AFM topography images of the blend films (Figure 3a,c,e,g). The root-mean-square (rms) surface roughness increases in the order of P3HT:PCBM (11.8 nm) < P3HT:mono-PCBOE (16.5 nm) < P3HT:bis-PCBOE (26.8 nm) < P3HT:tris-PCBOE (28.6 nm). The surface roughness may reflect the extent of P3HT self-organization, which can be promoted by thermal annealing,[54,55] solvent vapor annealing[56] and slow drying,[17] or by using solvent additives.[57] In addition, recent studies have shown that fullerene agglomerates protruding out of the film surfaces also largely contribute to the surface roughness.[58−60] In the present cases, the slow-drying treatment prior to thermal annealing retarded the film solidification, which in effect prolonged the crystallization of fullerenes, especially for those bearing more side substitutes.[61−63] This is responsible for the increase of surface roughness and is consistent with the picture of vertical phase separation in the P3HT:fullerene photoactive layers, as recently revealed by means of variable-angle spectroscopic ellipsometry (VASE)[64] and X-ray photoelectron spectroscopy (XPS)/AFM characterizations.[65]

As seen in the lower row of Figure 3, the blends show distinctly different phase contrasts. For all of the blends, the P3HT fibrillar crystallites appear as inhomogeneous textures, and the regions between fibrillars are filled up with fullerene aggregates and polymer−fullerene mixed phases.[66] For P3HT:PCBM (Figure 3b) and P3HT:mono-PCBOE (Figure 3d), the P3HT crystalline domains are densely and uniformly distributed, whereas for P3HT:bis-PCBOE (Figure 3f) and

dx.doi.org/10.1021/jp407990d | J. Phys. Chem. C 2013, 117, 25898−25907

Table 1. Reductive Half-Wave Potentials (E vs Ag/Ag$^+$), Onset Reduction Potentials (E_{red}^{on}), and LUMO Energy Levels (E_{LUMO}) of the Fullerene Adducts. Shifts of E and E_{LUMO} with Respect to PCBM Are Given in Parentheses

fullerenes	E_1 (V)[a]	E_2 (V)[a]	E_3 (V)[a]	E_{red}^{on} (V)	E_{LUMO} (eV)
PCBM	−1.07	−1.47	−1.97	−0.94	−3.77
mono-PCBOE	−1.12 (−0.05)	−1.52 (−0.05)	−2.03 (−0.06)	−0.97	−3.74 (0.03)
bis-PCBOE	−1.22 (−0.15)	−1.61 (−0.14)	−2.23 (−0.26)	−1.06	−3.65 (0.13)
tris-PCBOE	−1.31 (−0.24)	−1.72 (−0.25)		−1.15	−3.56 (0.18)

[a]E was calculated with $E = (E_{p,c} + E_{p,a})/2$, where $E_{p,c}$ and $E_{p,a}$ are cathodic and anodic peak potentials, respectively (cf. Figure 2).

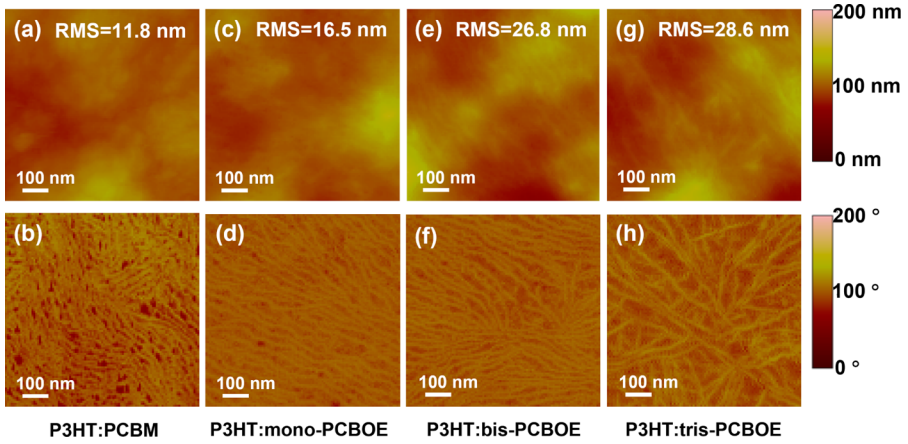

Figure 3. AFM topography (upper row) and phase images (lower row) of the blend films: (a,b) P3HT:PCBM, (c,d) P3HT:mono-PCBOE, (e,f) P3HT:bis-PCBOE, (g,h) P3HT:tris-PCBOE.

P3HT:tris-PCBOE (Figure 3h), the P3HT fibrilla become considerably sparser, suggesting severer fullerene agglomeration and the possible involvement of amorphous P3HT phases. Nevertheless, since in different types of blends the P3HT fibrilla networks have similar crystallinity, it is reasonable to attribute the variation of phase morphologies to the different extents of fullerene aggregation.

3.2. Device Performance. Figure 4a,b, respectively, show the $J-V$ curves and the EQE profiles of the PSCs, and the according device parameters are listed in Table 2. The devices based on PCBM, mono-PCBOE, bis-PCBOE, and tris-PCBOE exhibit increasingly higher V_{OC} (0.60 V < 0.61 V < 0.84 V < 0.87 V), correlating to the increase of E_{LUMO} as modified via substituting more electron-donating groups to the side chains of fullerene moieties.[26−28,31] To the opposite, these devices show rapidly decreased J_{SC} in the order of P3HT:PCBM (9.65 mA/cm^2) > P3HT:mono-PCBOE (5.83 mA/cm^2) > P3HT:bis-PCBOE (5.28 mA/cm^2) > P3HT:tris-PCBOE (1.87 mA/cm^2). It is known that J_{SC} depends mainly on the extent of light harvesting and the efficiency of charge photogeneration and transport. For light harvesting, all of the photoactive layers, 130−160 nm in thickness, are capable of fully absorbing the incident photons with the help of the Al-electrode reflection. On the other hand, the chemical potential of 0.82−1.00 eV provided by the fullerene-to-polymer LUMO level offsets are large enough to drive the interfacial exciton dissociation as proven by the >98% fluorescence quenching efficiency (Supporting Information, S4). Therefore, the substantial reduction in J_{SC} must be ascribed to the deficiency in free charge generation and extraction, which is supported by the monotonic decrease of FF, 0.67 (P3HT:PCBM) > 0.53 (P3HT:mono-PCBOE) > 0.50 (P3HT:bis-PCBOE) > 0.35 (P3HT:tris-PCBOE), and by the significant drop of electron mobility (μ_e) in this sequence (Table 2). Particularly, the μ_e of

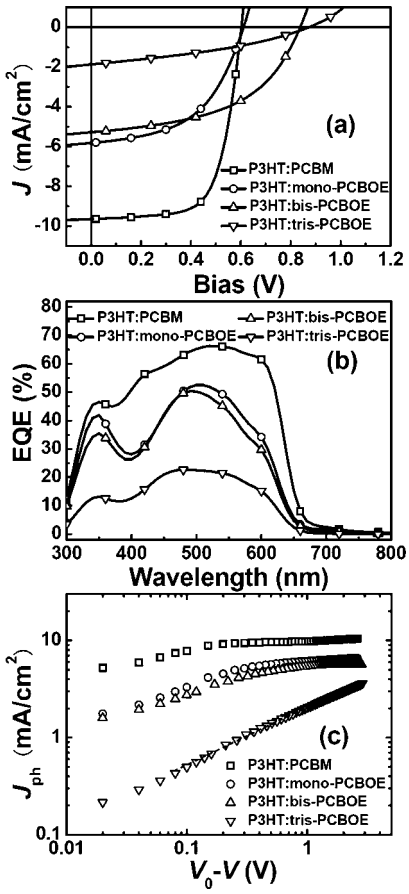

Figure 4. (a) $J-V$ curves, (b) EQE profiles, and (c) photocurrent-to-internal electrical bias ($V_0 - V$) dependence for the indicated P3HT:fullerene PSCs.

dx.doi.org/10.1021/jp407990d | J. Phys. Chem. C 2013, 117, 25898−25907

Table 2. Photovoltaic Performance of the PSCs, and Electron Mobilities of the Fullerene Adducts Determined from Respective Electron Single-Carrier Devices

devices	J_{SC} (mA/cm^2)	V_{OC} (V)	FF	PCE	μ_e (cm^2/(V s))
P3HT:PCBM	9.65 ± 0.15	0.60 ± 0.01	0.67 ± 0.01	3.90 ± 0.06	(5.0 ± 0.3) × 10^{-3}
P3HT:mono-PCBOE	5.83 ± 0.10	0.61 ± 0.01	0.53 ± 0.01	1.89 ± 0.04	(8.8 ± 0.4) × 10^{-4}
P3HT:bis-PCBOE	5.28 ± 0.09	0.84 ± 0.01	0.50 ± 0.01	2.22 ± 0.04	(2.6 ± 0.5) × 10^{-4}
P3HT:tris-PCBOE	1.87 ± 0.05	0.87 ± 0.01	0.35 ± 0.01	0.58 ± 0.02	(2.7 ± 0.4) × 10^{-7}

P3HT:tris-PCBOE (2.7×10^{-7} cm^2/(V s)), is about 3 orders of magnitude lower than the documented hole mobility of the P3HT:PCBM photoactive layer, $\mu_h = (1.4–3) \times 10^{-4}$ cm^2/(V s).[44,67] As discussed below, such largely unbalanced charge mobilities will lead to the space-charge limited extraction of charges.

In Figure 4b, the EQE profiles show apparent dips around 400 nm, which are relatively deeper in the cases of mono-PCBOE and bis-PCBOE. They are mostly likely due to the weak P3HT absorption at ~400 nm. Importantly, the EQEs at 600 nm decrease in the order of P3HT:PCBM (61%) > P3HT:mono-PCBOE (35%) > P3HT:bis-PCBOE (29%) > P3HT:tris-PCBOE (15%), which cannot be attributed to the variation of light absorptivity at ~600 nm, because the absorptivity at 600 nm is similar among different types of photoactive layers (cf. Figure 1). Rather, the EQE reduction for the PSCs based on higher adducts strongly indicates the increased loss of photocurrent via charge recombination, an issue which is to be verified by the time-resolved spectroscopic results.

Figure 4c plots the photocurrent density (J_{ph}) against the internal electrical bias ($V_0 - V$), where V_0 defines a compensation voltage at which the dark current meets the photocurrent.[68,69] In the regime of <0.1 V, all of the PSCs show linear J_{ph}-to-($V_0 - V$) dependence as a result of the competition between drifting and diffusive currents.[68] Above 0.1 V, the J_{ph} of the P3HT:tris-PCBOE device shows a square-root dependence on ($V_0 - V$), which together with the low FF unambiguously shows the accumulation of space charges.[67] The low μ_e and the resultant space charge accumulation were previously observed for the PSCs based on P3HT blended with other types of fullerene adducts.[30] To the contrary, the referencing P3HT:PCBM device exhibits the highest J_{SC} and FF owing to the well-balanced electron and hole mobilities. In the cases of P3HT:mono-PCBOE and P3HT:bis-PCBOE, the μ_e values as listed in Table 2 are comparable to the μ_h values of P3HT (~10^{-4} cm^2/(V s)); therefore, the photocurrents of these devices are charge-recombination limited rather than space-charge limited, as previously reported for other fullerene-adduct based PSCs.[70] In summary, it is concluded that electron and hole transport in the mono-PCBOE or the bis-PCBOE devices are approximately balanced, whereas those in the case of tris-PCBOE have to be considered as unbalanced.

3.3. Subnanosecond Charge Photogeneration Dynamics. To examine the effects of film morphology and charge mobilities on the dynamics of charge photogeneration, we carried out near-infrared time-resolved absorption measurement for the photoactive layers of P3HT blended with the fullerene adducts. The high detection sensitivity enables an excitation photon fluence as low as one-sun illumination, while the multicolor probe (850–1350 nm) allows clear differentiation of the exciton and the polaron of P3HT, which are hereafter denoted as P3HT* and P3HT$^{\bullet+}$, respectively.

3.3.1. Ultrafast Spectral Dynamics under Low Excitation Fluence. The ultrafast excitation and charge dynamics of thermally annealed or solvent-vapor annealed P3HT:PCBM blends had been investigated in detail,[49,71] on the basis of which the spectral dynamics of the P3HT:fullerene blends in Figure 5

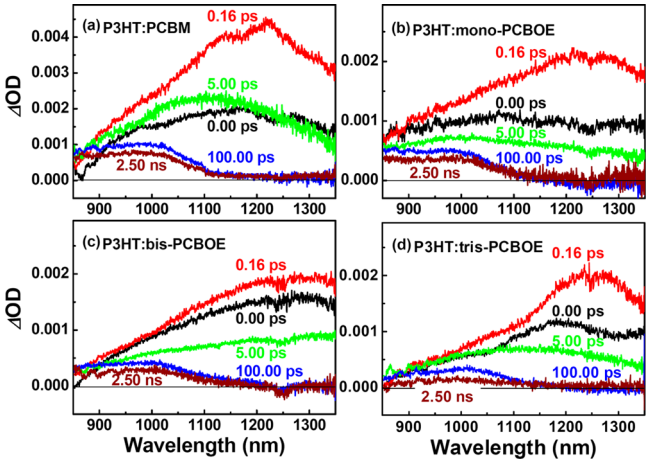

Figure 5. Transient spectra at selected delay times recorded following the photoexcitation at 620 nm. Excitation photon fluence was 4.0 × 10^{17} photons·cm^{-3}·pulse^{-1}.

are characterized below. It is evident by comparing Figure 5a–d that four different types of blends exhibit similar spectral dynamics: At Δt = 0.00 ps, they show broad absorption spectra peaking around 1200 nm, which are characteristic to the excited-state absorption of P3HT*. At Δt = 100 ps, the P3HT* absorption decay out completely owing to interfacial exciton dissociation and, later on, the transient spectra are dominated by the broad absorption in 850–1100 nm attributable to the P2 sub-band absorption (i.e., the SOMO-to-LUMO transition of P3HT$^{\bullet+}$).[49,71,72] Here, we note that the radical anion PCBM$^{\bullet-}$ with an absorption maximum at ~1020 nm may also contribute to the spectral regime of 850–1100 nm. However, the molar extinction coefficient of PCBM$^{\bullet-}$ ($\varepsilon_{1020\ nm} = 6 \times 10^3$ M^{-1} cm^{-1}) is substantially lower than that of P3HT$^{\bullet+}$ ($\varepsilon_{1000\ nm} = 3 \times 10^4$ M^{-1} cm^{-1}).[71,73,74] In addition, the later-phase (≥100 ps) transient features in Figure 5 differ completely from the monoband absorption signature of PCBM$^{\bullet-}$, whereas they agree well with the spectroelectrochemical spectra of P3HT$^{\bullet+}$.[49] These together with the relatively lower mixing ratio of fullerenes suggest negligible interference of PCBM$^{\bullet-}$ with the P3HT$^{\bullet+}$ absorption.

Under the low-fluence and red-edge photoexcitation at 620 nm, the P3HT* excitons migrate on a time scale of ~10 ps before being quenched via the P3HT–fullerene interfacial charge transfer reactions.[49,71] In the present cases, the time scale of exciton diffusion can be derived from the exciton kinetics at 1300 nm with minimized interference from P3HT$^{\bullet+}$ absorption. As shown in Figure 6, the exciton kinetics at 1300

dx.doi.org/10.1021/jp407990d | J. Phys. Chem. C 2013, 117, 25898–25907

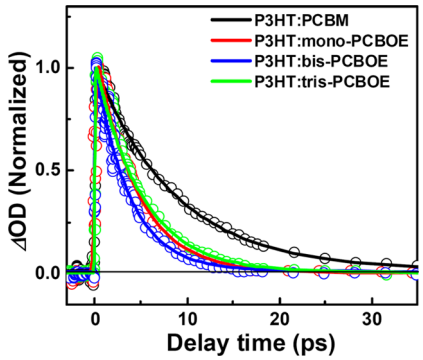

Figure 6. Normalized exciton kinetics at 1300 nm under the excitation photon fluences of 4.0 × 10^{17} photons·cm^{-3}·$pulse^{-1}$. Excitation wavelength was 620 nm. Solid lines are derived by fittings the kinetics curves to a monoexponential model function.

nm fit well to a monoexponential decay function. The decay time constants, 4.5 ± 0.1 ps for P3HT:mono-PCBOE, 3.7 ± 0.1 ps for P3HT:bis-PCBOE, and 5.0 ± 0.1 ps for P3HT:tris-PCBOE, are on average about half of that of P3HT:PCBM (8.7 ± 0.3 ps). It is known that the optical pulses at 620 nm preferentially excite the crystalline P3HT phase and that the intrinsic exciton lifetimes of neat P3HT films are ∼300 ps.[49] Therefore, in the blend films, the drastic reduction of exciton lifetimes must be due to the diffusion and the interfacial quenching of P3HT*. In addition, the rather similar P3HT crystallinity of four different types of blends (vide supra) suggest similar diffusion coefficients of P3HT* in these blends. Taking a typical exciton diffusion coefficient (D_e) of 2 × 10^{-3} cm^2 s^{-1},[75] the exciton diffusion lengths (L_D) of the different P3HT:PCBOE blends turn out to be 1.2−1.4 nm as estimated on the basis of the relation, $L_D = (2D_e\tau_1)^{1/2}$,[75] and the L_D dimensions of the P3HT:PCBOE blends are about 26% shrunken with respect to that of the P3HT:PCBM blend (1.9 nm). The L_D values thus estimated are comparable to those reported for the thermally annealed P3HT:PCBM films (1−2 nm).[71,76] The difference in L_D between the PCBOE and the PCBM blends may be related to the morphological scales (i.e., the P3HT crystalline domains of the PCBOE blends are smaller than those of the PCBM blend). In this context, the excitation delocalization length of P3HT* was reported to be ∼9 nm for thermally annealed P3HT:PCBM blends.[74] Therefore, assuming similar delocalization lengths of P3HT* of the four different types of blends in view of the similar P3HT crystallinity, the substantial reduction in the exciton lifetimes of the P3HT:PCBOE blends also suggest smaller P3HT crystalline domain sizes with reference to the P3HT:PCBM blend. In addition, the above comparison of P3HT* diffusion or delocalization lengths between the PCBOE and the PCBM blends imply relatively severer discontinuity of the P3HT crystalline phases in the PCBOE blends.

For convenience, we define from Figure 5 a relative $P3HT^{\bullet+}$ initial yield by taking an amplitude ratio of $\Delta OD_{1000\ nm}$ at Δt = 100 ps ($P3HT^{\bullet+}$ dominant) over $\Delta OD_{1200\ nm}$ at Δt = 0.16 ps (P3HT* dominant). The $P3HT^{\bullet+}$ yields thus obtained are comparable among the four different types of blend films (∼24%), indicating similar exciton migration and dissociation efficiencies of P3HT*. The uniform $P3HT^{\bullet+}$ yield correlates with the similar crystallinity of P3HT phases in different blends and accords to the selective photoexcitation of P3HT crystallites at 620 nm. However, the relative $P3HT^{\bullet+}$ yields at Δt = 2.5 ns, as the amplitude ratio of $\Delta OD_{1000\ nm}$ at Δt = 2.5 ns over $\Delta OD_{1200\ nm}$ at Δt = 0.16 ps, decrease in the order of P3HT:PCBM (18%) ≈ P3HT:mono-PCBOE (18%) > P3HT:bis-PCBOE (14%) > P3HT:tris-PCBOE (10%), suggesting accelerated charge recombination upon increasing the fullerene adduct order. This tendency correlates to the changes in morphology and electron mobility of the blend films as induced by the higher-order adducted fullerenes.

3.3.2. Influence of Excitation Photon Fluence on Polaron Kinetics. Figure 7 shows the $P3HT^{\bullet+}$ kinetics at 1000 nm

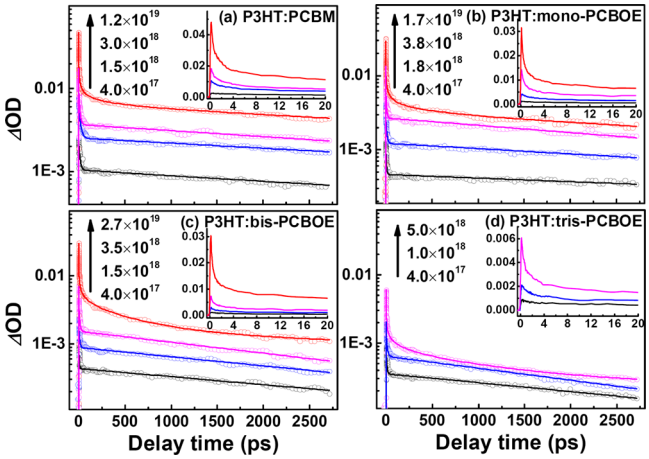

Figure 7. Semilogarithmic plot of the kinetics at 1000 nm under the indicated excitation photon fluences (in photons·cm^{-3}·$pulse^{-1}$; λ_{ex} = 620 nm). Solid lines are derived from curve fittings based on multiexponential or combined exponential and power-law model functions (see text for details). Insets show with linear coordination scales the initial phase of kinetics evolution (up to 20 ps).

recorded under various photon fluences. Comparing panels a−d, we see that the kinetics traces decay faster for a higher-order PCBOE adduct. In addition, when P3HT:bis-PCBOE (c) or P3HT:tris-PCBOE (d) are compared to P3HT:PCBM (a) or P3HT:mono-PCBOE (b), it is evident that the kinetics traces in (c) and (d) exhibit stronger photon-fluence dependence. Further kinetics differences are characterized below.

The kinetics traces for each blend can be categorized into two groups according to the applied photoexcitation fluences: (i) (Low fluence regime (10^{17} − ∼10^{18} photons·cm^{-3}·$pulse^{-1}$)). In Figure 7, for the respective blend films based on PCBM (a), mono-PCBOE (b), and bis-PCBOE (c), it is seen that later than 100 ps the low-fluence kinetics evolve almost parallel to each other. Such photon-fluence independence is characteristic to the geminate charge recombination. To the contrary, in Figure 7d, for tris-PCBOE the overall kinetics decay are distinctly faster compared to the other three cases, indicating faster charge recombination in the case of tris-PCBOE. (ii) (High fluence regime (∼10^{19} photons·cm^{-3}·$pulse^{-1}$)). In Figure 7a−d, at early delay times (0−20 ps), the fluence dependence of the kinetics are partially contributed by exciton−exciton annihilation and likely also by exciton-charge annihilation[77] as evidenced by the sublinear fluence dependence of the maximal ΔOD amplitude (Supporting Information, S5). Subsequently (>20 ps), when P3HT* essentially decayed out owing to the exciton dissociation and annihilation, the kinetics are dominated by $P3HT^{\bullet+}$. In the later regime (20−1500 ps), the high-fluence kinetics decay substantially faster than the low-fluence ones. Such photon-fluence dependence is

dx.doi.org/10.1021/jp407990d | J. Phys. Chem. C 2013, 117, 25898−25907

Table 3. Kinetics Parameters Obtained by Fitting the Kinetics at 1000 nm (cf. Figure 7) under Low Photon Fluence (10^{17} – $\sim10^{18}$ photons·cm^{-3}·pulse^{-1}) to $\Delta OD(t) = A_1\exp(-t/\tau_1) + A_2\exp(-t/\tau_2) + A_3\exp(-t/\tau_3)$ and Those under High Photon Fluence ($\sim10^{19}$ photons·cm^{-3}·pulse^{-1}) to $\Delta OD(t) = A_1\exp(-t/\tau_1) + A_2t^{-\alpha} + A_3\exp(-t/\tau_3)$. See Text for Details

		fitting parameters		
blend film	photon fluence (photons·cm^{-3}·pulse^{-1})	τ_1 (ps)	τ_2 (ps)	τ_3 (ns)
P3HT:PCBM	4.0×10^{17}	—	13.4 ± 0.4	6.2 ± 0.2
	1.5×10^{18}	1.4 ± 0.0	19.3 ± 0.5	7.2 ± 0.2
	3.0×10^{18}	0.8 ± 0.0	11.9 ± 0.2	6.0 ± 0.2
	1.2×10^{19}	1.1 ± 0.1	(α = 0.38 ± 0.02)	9.3 ± 1.0
P3HT:mono-PCBOE	4.0×10^{17}	—	6.4 ± 0.1	8.5 ± 0.4
	1.8×10^{18}	1.0 ± 0.0	10.8 ± 0.3	6.0 ± 0.2
	3.8×10^{18}	0.5 ± 0.0	7.9 ± 0.2	4.4 ± 0.1
	1.7×10^{19}	0.2 ± 0.0	(α = 0.33 ± 0.01)	5.3 ± 0.2
P3HT:bis-PCBOE	4.0×10^{17}	—	3.9 ± 0.1	3.7 ± 0.2
	1.5×10^{18}	0.6 ± 0.0	8.1 ± 0.4	3.1 ± 0.1
	3.5×10^{18}	0.4 ± 0.0	9.0 ± 0.3	2.7 ± 0.1
	2.7×10^{19}	0.2 ± 0.0	(α = 0.30 ± 0.01)	0.6 ± 0.0
P3HT:tris-PCBOE	4.0×10^{17}	—	7.3 ± 0.2	3.3 ± 0.1
	1.0×10^{18}	1.0 ± 0.0	11.9 ± 0.5	2.5 ± 0.1
	5.0×10^{18}	0.6 ± 0.0	(α = 0.30 ± 0.02)	1.1 ± 0.1

indicative of the involvement of nongeminate charge recombination resultant from the exaggerated photoexcitation fluence. Interestingly, the threshold of photon fluence inducing the nongeminate charge recombination is about an order of magnitude lower for the tris-PCBOE blend ($\sim10^{18}$ photons·cm^{-3}·pulse^{-1}) than those for the other blend films ($\sim10^{19}$ photons·cm^{-3}·pulse^{-1}), which can be related to the substantially low electron mobility and the space-charge accumulation in this case. More importantly, these results prove that the unbalanced charge transport causes detrimental nongeminate charge recombination, which is absent in the P3HT:PCBM and the P3HT:mono-PCBOE blends in the fluence regime up to $\sim10^{18}$ photons·cm^{-3}·pulse^{-1}.

The kinetics traces in Figure 7 were subjected to curve fitting, and the resultant kinetics parameters are listed in Table 3. For each of the blends, the kinetics in the aforementioned low and high photon fluence regimes, respectively, were fitted to different model functions depending on the underlying photophysics (i.e., geminate charge recombination for the low-fluence kinetics and nongeminate charge recombination for the high-fluence one. Under the lowest photon fluence (4×10^{17} photons·cm^{-3}·pulse^{-1}), the kinetics follow a biexponential decay function. The shorter decay time constants (τ_2) of the PCBOE blends (4–7 ps) are approximately half of that of the PCBM blend (13.4 ps), whereas the longer decay time constants (τ_3) are ascribed to the geminate recombination, which gets faster upon increasing the adduct order (i.e., mono-PCBOE (8.5 ns) > bis-PCBOE (3.7 ns) > tris-PCBOE (3.3 ns)). These nanosecond time scales are consistent with those reported for the P3HT/PCBM blends, ranging from a few to a few tens of nanoseconds.[77−80]

Under the moderately low photon fluence ($\sim10^{18}$ photons·cm^{-3}·pulse^{-1}), the kinetics traces fit well to a triexponential function. The first decay component (τ_1) on the time scales of subpicoseconds to a picosecond can be ascribed to the ultrafast annihilation of P3HT* before diffusion, which is evident in the insets of Figure 7, illustrating strong photon-fluence dependence of the picosecond kinetics. The second decay component (τ_2) on the time scales of ~10 ps are slightly longer than the time scales of exciton diffusion as determined from the low-fluence kinetics at 1300 nm (cf. Section 3.3.1). This is most likely due to the influence from the exciton annihilation, which in effect induces the formation of P3HT$^{\bullet+}$ via autoionizing the higher-lying excited state of P3HT.[81,82] The third decay component (τ_3) is on the time scale of sub-10 ns, which is ascribable to the geminate charge recombination reactions. Most importantly, on increasing the adduct order, these decay time constants (τ_3) decrease in the order of mono-PCBOE (4–7 ns) > bis-PCBOE (~3 ns) ~ tris-PCBOE (~3 ns), which is consistent with the trend of geminate charge recombination observed under the lowest fluence photoexcitation.

Under the highest applied photon fluence ($\sim10^{19}$ photons·cm^{-3}·pulse^{-1}), the kinetics traces of each case could not be fitted to a triexponential model function, instead, they can be well described by the model function combined exponential and power law components, $\Delta OD(t) = A_1\exp(-t/\tau_1) + A_2t^{-\alpha} + A_3\exp(-t/\tau_3)$ (Supporting Information S6). The power law (t-exponential) kinetics is known to be valid for describing the trap-limited hole recombination in polymer–PCBM blends.[83,84] Therefore, in view of the nongeminate behavior of the high-fluence kinetics, the incorporation of a t-exponential component is reasonable. As listed in Table 3, the nanosecond exponential decay component (τ_3) is close to or not far from the time constants of the geminate charge recombination mentioned above. Importantly, the power-law exponent (α) decreases from 0.38 (P3HT:PCBM) to 0.33 (P3HT:mono-PCBOE), and further to 0.30 (P3HT:bis-PCBOE and P3HT:tris-PCBOE) upon increasing the adduct order, implying that the reaction order of nongeminate charge recombination gets systematically higher (i.e., from 3.6 to 4.0, and further to 4.3). This is due to the substantially lower electron mobility of the P3HT:tris-PCBOE blend (μ_e, 2.7×10^{-7} cm^2/(V s)) than the hole mobility of thermally annealed P3HT:PCBM blends (μ_h, $(1.4–3) \times 10^{-4}$ cm^2/(V s))[44,67] and the resultant imbalance of ambipolar charge transport as reflected by the SCLC data (Figure 4c). Thus the space-charge limited charge transport arisen from the discontinuity in P3HT and/or fullerene crystalline phases introduced severe nongeminate recombination in the case of tris-PCBOE, which in turn largely deteriorated the J–V performance (Figure 4a).

dx.doi.org/10.1021/jp407990d | J. Phys. Chem. C 2013, 117, 25898–25907

4. SUMMARY

With reference to PCBM, the newly synthesized PCBOEs in combination with P3HT effectively enhanced the V_{OC} but deteriorated the J_{SC} and the FFs of the P3HT-PCBOE PSCs. Similar device performance of different types of fullerene multiadducts had been reported previously.[85−87] The present work is intended to seek for the possible limiting factors of photocurrent with an emphasize on the effects of adduct order.

On the basis of systematic studies of the photoactive-layer morphologies and the primary exciton and polaron dynamics, we have shown that, under similar thermal-annealing conditions of the photoactive layers, a PCBOE of higher adduct order aggregates to a higher extent and interferes more with the crystalline textures of the P3HT network. Such morphological variation impacts intimately on the primary photogeneration and the transport of charge carriers: (i) As a major photocurrent loss mechanism, geminate charge recombination for the bis-PCBOE and the tris-PCBOE blends (3−4 ns) are 2-fold faster than those of the mono-PCBOE and the PCBM blends (6−8 ns); geminate recombination can be a major photocurrent loss mechanism when higher order fullerene adducts are employed. (ii) In the case of tris-PCBOE subjected to moderately low fluence photoexcitation, nongeminate charge recombination, not seen in the mono-PCBOE or PCBM blends, comes into play as an additional mechanism of photocurrent loss. The occurrence of nongeminate charge recombination in the tris-PCBOE blend observed on a nanosecond time scale is ascribed to the space-charge limited charge transport, which is originated from the three-orders-of-magnitude deteriorated electron mobility (compared to the mono-PCBOE blend) as a consequence of the polymer- and/or fullerene-phase discontinuity.

The present work shows that, on increasing the fullerene adduct order, the transport of positive and negative charges in the corresponding photoactive layers turns from ambipolarly balanced to space-charge limited states. For practical usages of multiadducted fullerenes in PSCs, the geminate and the nongeminate charge recombination are critical photocurrent loss mechanisms. However, such photocurrent loss can be effectively minimized via optimizing the polymer-fullerene biphasic morphologies of the BHJ layers to maintain balanced charge transport. Since the solvent solubility and the polymer miscibility of fullerene multiadducts are different from those of PCBM, it is promising to simultaneously boost the photovoltage and photocurrent of PSCs by the use of fullerene multiadducts, which may be brought about by the BHJ morphology optimization using specific solvent systems and annealing protocols.

■ ASSOCIATED CONTENT

Ⓢ Supporting Information

^{1}H- and ^{13}C NMR, FTIR and MS (MALDI-TOF) data for structural characterization, XRD characterization and fluorescence quenching efficiency of blend films, photon-fluence dependence of ΔOD amplitude, additional curve fitting results. This information is available free of charge via the Internet at http://pubs.acs.org.

■ AUTHOR INFORMATION

Corresponding Author

*E-mail: jpzhang@chem.ruc.edu.cn (J.-P.Z.). Fax: +86-10-62516444. Tel: +86-10-62516604.

Notes

The authors declare no competing financial interest.

■ ACKNOWLEDGMENTS

Grant-in-aid from the Natural Science Foundation of China (No. 20933010) is acknowledged. We are indebted to Dr. L. Guan and Prof. Z.-X. Guo for their help in the morphological and the structural characterizations.

■ REFERENCES

(1) Yu, G.; Gao, J.; Hummelen, J. C.; Wudl, F.; Heeger, A. J. Polymer Photovoltaic Cells: Enhanced Efficiencies via a Network of Internal Donor-Acceptor Heterojunctions. *Science* **1995**, *270*, 1789−1791.

(2) Günes, S.; Neugebauer, H.; Sariciftci, N. S. Conjugated Polymer-Based Organic Solar Cells. *Chem. Rev.* **2007**, *107*, 1324−1338.

(3) Thompson, B. C.; Fréchet, J. M. J. Polymer−Fullerene Composite Solar Cells. *Angew. Chem., Int. Ed.* **2008**, *47*, 58−77.

(4) Dennler, G.; Scharber, M. C.; Brabec, C. J. Polymer-Fullerene Bulk-Heterojunction Solar Cells. *Adv. Mater.* **2009**, *21*, 1323−1338.

(5) Cheng, Y.-J.; Yang, S.-H.; Hsu, C.-S. Synthesis of Conjugated Polymers for Organic Solar Cell Applications. *Chem. Rev.* **2009**, *109*, 5868−5923.

(6) Delgado, J. L.; Bouit, P.-A.; Filippone, S.; Herranza, M. Á.; Martín, N. Organic Photovoltaics: A Chemical Approach. *Chem. Commun.* **2010**, *46*, 4853−4865.

(7) Li, C.; Liu, M.; Pschirer, N. G.; Baumgarten, M.; Müllen, K. Polyphenylene-Based Materials for Organic Photovoltaics. *Chem. Rev.* **2010**, *110*, 6817−6855.

(8) Boudreault, P.-L. T.; Najari, A.; Leclerc, M. Processable Low-Bandgap Polymers for Photovoltaic Applications. *Chem. Mater.* **2011**, *23*, 456−469.

(9) Li, G.; Zhu, R.; Yang, Y. Polymer Solar Cells. *Nat. Photon.* **2012**, *6*, 153−161.

(10) Li, Y. Molecular Design of Photovoltaic Materials for Polymer Solar Cells: Toward Suitable Electronic Energy Levels and Broad Absorption. *Acc. Chem. Res.* **2012**, *45*, 723−733.

(11) Peet, J.; Kim, J. Y.; Coates, N. E.; Ma, W. L.; Moses, D.; Heeger, A. J.; Bazan, G. C. Efficiency Enhancement in Low-Bandgap Polymer Solar Cells by Processing with Alkane Dithiols. *Nat. Mater.* **2007**, *6*, 497−500.

(12) Chen, H.-Y.; Hou, J.; Zhang, S.; Liang, Y.; Yang, G.; Yang, Y.; Yu, L.; Wu, Y.; Li, G. Polymer Solar Cells with Enhanced Open-Circuit Voltage and Efficiency. *Nat. Photon.* **2009**, *3*, 649−653.

(13) Liang, Y.; Xu, Z.; Xia, J.; Tsai, S.-T.; Wu, Y.; Li, G.; Ray, C.; Yu, L. For the Bright Future—Bulk Heterojunction Polymer Solar Cells with Power Conversion Efficiency of 7.4%. *Adv. Mater.* **2010**, *22*, E135−E138.

(14) He, Z.; Zhong, C.; Su, S.; Xu, M.; Wu, H.; Cao, Y. Enhanced Power-Conversion Efficiency in Polymer Solar Cells Using an Inverted Device Structure. *Nat. Photon.* **2012**, *6*, 591−595.

(15) Ma, W.; Yang, C.; Gong, X.; Lee, K.; Heeger, A. J. Thermally Stable, Efficient Polymer Solar Cells with Nanoscale Control of the Interpenetrating Network Morphology. *Adv. Funct. Mater.* **2005**, *15*, 1617−1622.

(16) Kim, J. Y.; Kim, S. H.; Lee, H.-Ho; Lee, K.; Ma, W.; Gong, X.; Heeger, A. J. New Architecture for High-Efficiency Polymer Photovoltaic Cells Using Solution-Based Titanium Oxide as an Optical Spacer. *Adv. Mater.* **2006**, *18*, 572−576.

(17) Li, G.; Shrotriya, V.; Huang, J.; Yao, Y.; Moriarty, T.; Emery, K.; Yang, Y. High-Efficiency Solution Processable Polymer Photovoltaic Cells by Self-Organization of Polymer Blends. *Nat. Mater.* **2005**, *4*, 864−868.

(18) Reyes-Reyes, M.; Kim, K.; Carroll, D. L. High-Efficiency Photovoltaic Devices Based on Annealed Poly(3-hexylthiophene) and 1-(3-Methoxycarbonyl)-propyl-1-phenyl-(6,6)C_{61} Blends. *Appl. Phys. Lett.* **2005**, *87*, 083506.

(19) Kim, Y.; Cook, S.; Tuladhar, S. M.; Choulis, S. A.; Nelson, J.; Durrant, J. R.; Bradley, D. D. C.; Giles, M.; McCulloch, I.; Ha, C.-S.;

et al. A Strong Regioregularity Effect in Self-Organizing Conjugated Polymer Films and High-Efficiency Polythiophene:Fullerene Solar Cells. *Nat. Mater.* **2006**, *5*, 197−203.
(20) Guo, X.; Cui, C.; Zhang, M.; Huo, L.; Huang, Y.; Hou, J.; Li, Y. High Efficiency Polymer Solar Cells Based on Poly(3-hexylthiophene)/Indene-C_{70} Bisadduct with Solvent Additive. *Energy Environ. Sci.* **2012**, *5*, 7943−7949.
(21) Yang, X.; Loos, J.; Veenstra, S. C.; Verhees, W. J. H.; Wienk, M. M.; Kroon, J. M.; Michels, M. A. J.; Janssen, R. A. J. Nanoscale Morphology of High-Performance Polymer Solar Cells. *Nano Lett.* **2005**, *5*, 579−583.
(22) Dang, M. T.; Hirsch, L.; Wantz, G.; Wuest, J. D. Controlling the Morphology and Performance of Bulk Heterojunctions in Solar Cells. Lessons Learned from the Benchmark Poly(3-hexylthiophene):[6,6]-Phenyl-C_{61}-butyric Acid Methyl Ester System. *Chem. Rev.* **2013**, *113*, 3734−3765.
(23) Brabec, C. J.; Cravino, A.; Meissner, D.; Sariciftci, N. S.; Fromherz, T.; Rispens, M. T.; Sanchez, L.; Hummelen, J. C. Origin of the Open Circuit Voltage of Plastic Solar Cells. *Adv. Funct. Mater.* **2001**, *11*, 374−380.
(24) Scharber, M. C.; Mühlbacher, D.; Koppe, M.; Denk, P.; Waldauf, C.; Heeger, A. J.; Brabec, C. J. Design Rules for Donors in Bulk-Heterojunction Solar Cells—Towards 10% Energy-Conversion Efficiency. *Adv. Mater.* **2006**, *18*, 789−794.
(25) Koster, L. J. A.; Mihailetchi, V. D.; Blom, P. W. M. Ultimate Efficiency of Polymer Fullerene Bulk Heterojunction Solar Cells. *Appl. Phys. Lett.* **2006**, *88*, 093511.
(26) Kooistra, F. B.; Knol, J.; Kastenberg, F.; Popescu, L. M.; Verhees, W. J. H.; Kroon, J. M.; Hummelen, J. C. Increasing the Open Circuit Voltage of Bulk-Heterojunction Solar Cells by Raising the LUMO Level of the Acceptor. *Org. Lett.* **2007**, *9*, 551−554.
(27) Backer, S. A.; Sivula, K.; Kavulak, D. F.; Fréchet, J. M. J. High Efficiency Organic Photovoltaics Incorporating a New Family of Soluble Fullerene Derivatives. *Chem. Mater.* **2007**, *19*, 2927−2929.
(28) Yang, C.; Kim, J. Y.; Cho, S.; Lee, J. K.; Heeger, A. J.; Wudl, F. Functionalized Methanofullerenes Used as n-Type Materials in Bulk-Heterojunction Polymer Solar Cells and in Field-Effect Transistors. *J. Am. Chem. Soc.* **2008**, *130*, 6444−6450.
(29) Lenes, M.; Wetzelaer, G.-J. A. H.; Kooistra, F. B.; Veenstra, S. C.; Hummelen, J. C.; Blom, P. W. M. Fullerene Bisadducts for Enhanced Open-Circuit Voltages and Efficiencies in Polymer Solar Cells. *Adv. Mater.* **2008**, *20*, 2116−2119.
(30) Lenes, M.; Shelton, S. W.; Sieval, A. B.; Kronholm, D. F.; Hummelen, J. C.; Blom, P. W. M. Electron Trapping in Higher Adduct Fullerene-Based Solar Cells. *Adv. Funct. Mater.* **2009**, *19*, 3002−3007.
(31) Choi, J. H.; Son, K.-I.; Kim, T.; Kim, K.; Ohkubo, K.; Fukuzumi, S. Thienyl-Substituted Methanofullerene Derivatives for Organic Photovoltaic Cells. *J. Mater. Chem.* **2010**, *20*, 475−482.
(32) He, Y.; Chen, H.-Y.; Hou, J.; Li, Y. Indene-C_{60} Bisadduct: A New Acceptor for High-Performance Polymer Solar Cells. *J. Am. Chem. Soc.* **2010**, *132*, 1377−1382.
(33) Zhao, G.; He, Y.; Li, Y. 6.5% Efficiency of Polymer Solar Cells Based on Poly(3-hexylthiophene) and Indene-C_{60} Bisadduct by Device Optimization. *Adv. Mater.* **2010**, *22*, 4355−4358.
(34) Ross, R. B.; Cardona, C. M.; Guldi, D. M.; Sankaranarayanan, S. G.; Reese, M. O.; Kopidakis, N.; Peet, J.; Walker, B.; Bazan, G. C.; Keuren, E. V. Endohedral Fullerenes for Organic Photovoltaic Devices. *Nat. Mater.* **2009**, *8*, 208−212.
(35) Cheng, Y.-J.; Liao, M.-H.; Chang, C.-Y.; Kao, W.-S.; Wu, C.-E.; Hsu, C.-S. Di(4-methylphenyl)methano-C_{60} Bis-Adduct for Efficient and Stable Organic Photovoltaics with Enhanced Open-Circuit Voltage. *Chem. Mater.* **2011**, *23*, 4056−4062.
(36) Mikroyannidis, J. A.; Kabanakis, A. N.; Sharma, S. S.; Sharma, G. D. A Simple and Effective Modification of PCBM for Use as an Electron Acceptor in Efficient Bulk Heterojunction Solar Cells. *Adv. Funct. Mater.* **2011**, *21*, 746−755.
(37) Xin, H.; Subramaniyan, S.; Kwon, T.-W.; Shoaee, S.; Durrant, J. R.; Jenekhe, S. A. Enhanced Open Circuit Voltage and Efficiency of Donor-Acceptor Copolymer Solar Cells by Using Indene-C_{60} Bisadduct. *Chem. Mater.* **2012**, *24*, 1995−2001.
(38) He, Y.; You, J.; Dou, L.; Chen, C.-C.; Richard, E.; Cha, K. C.; Wu, Y.; Li, G.; Yang, Y. High Performance Low Band Gap Polymer Solar Cells with a Non-conventional Acceptor. *Chem. Commun.* **2012**, *48*, 7616−7618.
(39) Troshin, P. A.; Hoppe, H.; Renz, J.; Egginger, M.; Mayorova, J. Y.; Goryachev, A. E.; Peregudov, A. S.; Lyubovskaya, R. N.; Gobsch, G.; Sariciftci, N. S.; et al. Material Solubility-Photovoltaic Performance Relationship in the Design of Novel Fullerene Derivatives for Bulk Heterojunction Solar Cells. *Adv. Funct. Mater.* **2009**, *19*, 779−788.
(40) Kim, K.-H.; Kang, H.; Kim, H. J.; Kim, P. S.; Yoon, S. C.; Kim, B. J. Effects of Solubilizing Group Modification in Fullerene Bis-Adducts on Normal and Inverted Type Polymer Solar Cells. *Chem. Mater.* **2012**, *24*, 2373−2381.
(41) Treat, N. D.; Varotto, A.; Takacs, C. J.; Batara, N.; Al-Hashimi, M.; Heeney, M. J.; Heeger, A. J.; Wudl, F.; Hawker, C. J.; Chabinyc, M. L. Polymer-Fullerene Miscibility: A Metric for Screening New Materials for High-Performance Organic Solar Cells. *J. Am. Chem. Soc.* **2012**, *134*, 15869−15879.
(42) Faist, M. A.; Keivanidis, P. E.; Foster, S.; Woebkenberg, P. H.; Anthopoulos, T. D.; Bradley, D. D. C.; Durrant, J. R.; Nelson, J. Effect of Multiple Adduct Fullerenes on Charge Generation and Transport in Photovoltaic Blends with Poly(3-hexylthiophene-2,5-diyl). *J. Polym. Sci., Part B: Polym. Phys.* **2011**, *49*, 45−51.
(43) Nuzzo, D. D.; Wetzelaer, G. A. H.; Bouwer, R. K. M.; Gevaerts, V. S.; Meskers, S. C. J.; Hummelen, J. C.; Blom, P. W. M.; Janssen, R. A. J. Simultaneous Open-Circuit Voltage Enhancement and Short-Circuit Current Loss in Polymer:Fullerene Solar Cells Correlated by Reduced Quantum Efficiency for Photoinduced Electron. *Adv. Energy. Mater.* **2013**, *3*, 85−94.
(44) Faist, M. A.; Shoaee, S.; Tuladhar, S.; Dibb, G. F. A.; Foster, S.; Gong, W.; Kirchartz, T.; Bradley, D. D. C.; Durrant, J. R.; Nelson, J. Understanding the Reduced Efficiencies of Organic Solar Cells Employing Fullerene Multiadducts as Acceptors. *Adv. Energy Mater.* **2013**, *3*, 744−752.
(45) Shoaee, S.; Subramaniyan, S.; Xin, H.; Keiderling, C.; Tuladhar, P. S.; Jamieson, F.; Jenekhe, S. A.; Durrant, J. R. Charge Photogeneration for a Series of Thiazolo−Thiazole Donor Polymers Blended with the Fullerene Electron Acceptors PCBM and ICBA. *Adv. Funct. Mater.* **2013**, *23*, 3286−3298.
(46) Hummelen, J. C.; Knight, B. W.; LePeq, F.; Wudl, F.; Yao, J.; Wilkins, C. L. Preparation and Characterization of Fulleroid and Methanofullerene Derivatives. *J. Org. Chem.* **1995**, *60*, 532−538.
(47) Jiang, C. Y.; Sun, X. W.; Zhao, D. W.; Kyaw, A. K. K.; Li, Y. N. Low Work Function Metal Modified ITO as Cathode for Inverted Polymer Solar Cells. *Sol. Energy Mater. Sol. Cells* **2010**, *94*, 1618−1621.
(48) Blom, P. W. M.; Mihailetchi, V. D.; Koster, L. J. A.; Markov, D. E. Device Physics of Polymer:Fullerene Bulk Heterojunction Solar Cells. *Adv. Mater.* **2007**, *19*, 1551−1566.
(49) Zhang, W.; Hu, R.; Li, D.; Huo, M.-M.; Ai, X.-C.; Zhang, J.-P. Primary Dynamics of Exciton and Charge Photogeneration in Solvent Vapor Annealed P3HT/PCBM Films. *J. Phys. Chem. C* **2012**, *116*, 4298−4310.
(50) Zhang, W.; Wang, Y.-W.; Hu, R.; Fu, L.-M.; Ai, X.-C.; Zhang, J.-P.; Hou, J.-H. Mechanism of Primary Charge Photogeneration in Polyfluorene Copolymer/Fullerene Blends and Influence of the Donor/Acceptor Lowest Unoccupied Molecular Orbital Level Offset. *J. Phys. Chem. C* **2013**, *117*, 735−749.
(51) Peet, J.; Senatore, M. L.; Heeger, A. J.; Bazan, G. C. The Role of Processing in the Fabrication and Optimization of Plastic Solar Cells. *Adv. Mater.* **2009**, *21*, 1521−1527.
(52) Eiermann, M.; Haddon, R. C.; Knight, B.; Li, Q. C.; Maggini, M.; Martín, N.; Ohno, T.; Prato, M.; Suzuki, T.; Wudl, F. Electrochemical Evidence for Through-Space Orbital Interactions in Spiromethanofullerenes. *Angew. Chem., Int. Ed.* **1995**, *34*, 1591−1594.
(53) Sun, Q.; Wang, H.; Yang, C.; Li, Y. Synthesis and Electroluminescence of Novel Copolymers Containing Crown Ether Spacers. *J. Mater. Chem.* **2003**, *13*, 800−806.

(54) Erb, T.; Zhokhavets, U.; Gobsch, G.; Raleva, S.; Stühn, B.; Schilinsky, P.; Waldauf, C.; Brabec, C. J. Correlation Between Structural and Optical Properties of Composite Polymer/Fullerene Films for Organic Solar Cells. *Adv. Funct. Mater.* **2005**, *15*, 1193−1196.
(55) Hoppe, H.; Sariciftci, N. S. Morphology of Polymer/Fullerene Bulk Heterojunction Solar Cells. *J. Mater. Chem.* **2006**, *16*, 45−61.
(56) Li, G.; Yao, Y.; Yang, H.; Shrotriya, V.; Yang, G.; Yang, Y. "Solvent Annealing" Effect in Polymer Solar Cells Based on Poly(3-hexylthiophene) and Methanofullerenes. *Adv. Funct. Mater.* **2007**, *17*, 1636−1644.
(57) Yao, Y.; Hou, J.; Xu, Z.; Li, G.; Yang, Y. Effects of Solvent Mixtures on the Nanoscale Phase Separation in Polymer Solar Cells. *Adv. Funct. Mater.* **2008**, *18*, 1783−1789.
(58) Chirvase, D.; Parisi, J.; Hummelen, J. C.; Dyakonov, V. Influence of Nanomorphology on the Photovoltaic Action of Polymer-Fullerene Composites. *Nanotechnology* **2004**, *15*, 1317−1323.
(59) Klimov, E.; Li, W.; Yang, X.; Hoffmann, G. G; Loos, J. Scanning Near-Field and Confocal Raman Microscopic Investigation of P3HT-PCBM Systems for Solar Cell Applications. *Macromolecules* **2006**, *39*, 4493−4496.
(60) Swinnen, A.; Haeldrmans, I.; vande Ven, M.; D'Haen, J.; Vanhoyland, G.; Aresu, S.; D'Olieslaeger, M.; Manca, J. Tuning the Dimensions of C_{60}-Based Needlelike Crystals in Blended Thin Films. *Adv. Funct. Mater.* **2006**, *16*, 760−765.
(61) Chang, C.-L.; Liang, C.-W.; Syu, J.-J.; Wang, L.; Leung, M.-K. Triphenylamine-Substituted Methanofullerene Derivatives for Enhanced Open-Circuit Voltages and Efficiencies in Polymer Solar Cells. *Sol. Energy Mater. Sol. Cells* **2011**, *95*, 2371−2379.
(62) Guilbert, A. A. Y.; Reynolds, L. X.; Bruno, A.; MacLachlan, A.; King, S. P.; Faist, M. A.; Pires, E.; Macdonald, J. E.; Stingelin, N.; Haque, S. A.; et al. Effect of Multiple Adduct Fullerenes on Microstructure and Phase Behavior of P3HT:Fullerene Blend Films for Organic Solar Cells. *ACS Nano* **2012**, *5*, 3868−3875.
(63) Azimi, H.; Fournier, D.; Wirix, M.; Dobrocka, E.; Ameri, T.; Machui, F.; Rodman, S.; Dennler, G.; Scharber, M. C.; Hingerl, K.; et al. Nano-Morphology Characterization of Organic Bulk Heterojunctions Based on Mono and Bis-Adduct Fullerenes. *Org. Electron.* **2012**, *13*, 1315−1321.
(64) Campoy-Quiles, M.; Ferenczi, T.; Agostinelli, T.; Etchegoin, P. G.; Kim, Y.; Anthopoulos, T. D.; Stavrinou, P. N.; Bradley, D. D. C.; Nelson, J. Morphology Evolution via Self-Organization and Lateral and Vertical Diffusion in Polymer Fullerene Solar Cell Blends. *Nat. Mater.* **2008**, *7*, 158−164.
(65) Xu, Z.; Chen, L.-M.; Yang, G.; Huang, C.-H.; Hou, J.; Wu, Y.; Li, G.; Hsu, C.-S.; Yang, Y. Vertical Phase Separation in Poly(3-hexylthiophene):Fullerene Derivative Blends and its Advantage for Inverted Structure Solar Cells. *Adv. Funct. Mater.* **2009**, *19*, 1227−1234.
(66) Shrotriya, V.; Yao, Y.; Li, G.; Yang, Y. Effect of Self-Organization in Polymer/Fullerene Bulk Heterojunctions on Solar Cell Performance. *Appl. Phys. Lett.* **2006**, *89*, 063505.
(67) Mihailetchi, V. D.; Xie, H.; Bert de, Boer; Koster, L. J. A.; Blom, P. W. M. Charge Transport and Photocurrent Generation in Poly(3-hexylthiophene):Methanofullerene Bulk-Heterojunction Solar Cells. *Adv. Funct. Mater.* **2006**, *16*, 699−708.
(68) Mihailetchi, V. D.; Koster, L. J. A.; Hummelen, J. C.; Blom, P. W. M. Photocurrent Generation in Polymer−Fullerene Bulk Heterojunctions. *Phys. Rev. Lett.* **2004**, *93*, 216601.
(69) Mihailetchi, V. D.; Wildeman, J.; Blom, P. W. M. Space-Charge Limited Photocurrent. *Phys. Rev. Lett.* **2005**, *94*, 126602.
(70) Azimi, H.; Senes, A.; Scharber, M. C.; Hingerl, K.; Brabec, C. J. Charge Transport and Recombination in Low-Bandgap Bulk Heterojunction Solar Cell Using Bis-Adduct Fullerene. *Adv. Energy Mater.* **2011**, *1*, 1162−1168.
(71) Guo, J.; Ohkita, H.; Benten, H.; Ito, S. Charge Generation and Recombination Dynamics in Poly(3-hexylthiophene)/Fullerene Blend Films with Different Regioregularities and Morphologies. *J. Am. Chem. Soc.* **2010**, *132*, 6154−6164.
(72) Jiang, X. M.; Österbacka, R.; Korovyanko, O.; An, C. P.; Horovitz, B.; Janssen, R. A. J.; Vardeny, Z. V. Spectroscopic Studies of Photoexcitations in Regioregular and Regiorandom Polythiophene Films. *Adv. Funct. Mater.* **2002**, *12*, 587−597.
(73) Yamamoto, S.; Guo, J.; Ohkita, H.; Ito, S. Formation of Methanofullerene Cation in Bulk Heterojunction Polymer Solar Cells Studied by Transient Absorption Spectroscopy. *Adv. Funct. Mater.* **2008**, *18*, 2555−2562.
(74) Guo, J.; Ohkita, H.; Benten, H.; Ito, S. Near-IR Femtosecond Transient Absorption Spectroscopy of Ultrafast Polaron and Triplet Exciton Formation in Polythiophene Films with Different Regioregularities. *J. Am. Chem. Soc.* **2009**, *131*, 16869−16880.
(75) Shaw, P. E.; Ruseckas, A.; Samuel, I. D. W. Exciton Diffusion Measurements in Poly(3-hexylthiophene). *Adv. Mater.* **2008**, *20*, 3516−3520.
(76) Marsh, R. A.; Hodgkiss, J. M.; Albert-Seifried, S.; Friend, R. H. Effect of Annealing on P3HT:PCBM Charge Transfer and Nanoscale Morphology Probed by Ultrafast Spectroscopy. *Nano Lett.* **2010**, *10*, 923−930.
(77) Howard, I. A.; Mauer, R.; Meister, M.; Laquai, F. Effect of Morphology on Ultrafast Free Carrier Generation in Polythiophene:-Fullerene Organic Solar Cells. *J. Am. Chem. Soc.* **2010**, *132*, 14866−14876.
(78) Meskers, S. C. J.; van Hal, P. A.; Spiering, A. J. H.; Hummelen, J. C.; van der Meer, A. F. G.; Janssen, R. A. J. Time-Resolved Infrared-Absorption Study of Photoinduced Charge Transfer in a Polythiophene-Methanofullerene Composite Film. *Phys. Rev. B* **2000**, *61*, 9917−9920.
(79) Hwang, I. W.; Moses, D.; Heeger, A. J. Photoinduced Carrier Generation in P3HT/PCBM Bulk Heterojunction Materials. *J. Phys. Chem. C* **2008**, *112*, 4350−4354.
(80) Clarke, T. M.; Durrant, J. R. Charge Photogeneration in Organic Solar Cells. *Chem. Rev.* **2010**, *110*, 6736−6767.
(81) Birks, J. B. *Organic Molecular Photophysics*; John Wiley & Sons: London, 1973.
(82) Dicker, G.; de Haas, M. P.; Siebbeles, L. D. A.; Warman, J. M. Electrodeless Time-Resolved Microwave Conductivity Study of Charge-Carrier Photogeneration in Regioregular Poly(3-hexylthiophene) Thin Films. *Phys. Rev. B* **2004**, *70*, 045203.
(83) Nogueira, A. F.; Montanari, I.; Nelson, J.; Durrant, J. R.; Winder, C.; Sariciftci, N. S.; Brabec, C. Charge Recombination in Conjugated Polymer/Fullerene Blended Films Studied by Transient Absorption Spectroscopy. *J. Phys. Chem. B* **2003**, *107*, 1567−1573.
(84) Clarke, T. M.; Jamieson, F. C.; Durrant, J. R. Transient Absorption Studies of Bimolecular Recombination Dynamics in Polythiophene/Fullerene Blend Films. *J. Phys. Chem. C* **2009**, *113*, 20934−20941.
(85) Faist, M. A.; Kirchartz, T.; Gong, W.; Ashraf, R. S.; McCulloch, I.; de Mello, J. C.; Ekins-Daukes, N. J.; Bradley, D. D. C.; Nelson, J. Competition between the Charge Transfer State and the Singlet States of Donor or Acceptor Limiting the Efficiency in Polymer:Fullerene Solar Cells. *J. Am. Chem. Soc.* **2012**, *134*, 685−692.
(86) Yamamoto, S.; Orimo, A.; Ohkita, H.; Benten, H.; Ito, S. Molecular Understanding of the Open-Circuit Voltage of Polymer:-Fullerene Solar Cells. *Adv. Energy. Mater.* **2012**, *2*, 229−237.
(87) Miller, N. C.; Sweetnam, S.; Hoke, E. T.; Gysel, R.; Miller, C. E.; Bartelt, J. A.; Xie, X.; Toney, M. F.; McGehee, M. D. Molecular Packing and Solar Cell Performance in Blends of Polymers with a Bisadduct Fullerene. *Nano Lett.* **2012**, *12*, 1566−1570.